

Semidiscrete vortex solitons

Xiaoxi Xu^{1§}, Guanghao Ou^{1§}, Zhaopin Chen², Bin Liu¹, Boris A. Malomed^{2,3}, Weicheng Chen¹, and Yongyao Li^{1,2*}

¹*School of Physics and Optoelectronic Engineering, Foshan University, Foshan 528000, China*

²*Department of Physical Electronics, School of Electrical Engineering,
Faculty of Engineering, and Center for Light-Matter Interaction,
Tel Aviv University, P.O.B. 39040, Tel Aviv, Israel*

³*Instituto de Alta Investigación, Universidad de Tarapacá, Casilla 7D, Arica, Chile*

§*These two authors contribute equally to this paper*

We demonstrate a possibility of creation of stable optical solitons combining one continuous and one discrete coordinates, with embedded vorticity, in an array of planar waveguides with intrinsic cubic-quintic nonlinearity. The same system may be realized in terms of the spatiotemporal light propagation in an array of tunnel-coupled optical fibers with the cubic-quintic nonlinearity. In contrast with zero-vorticity states, semidiscrete vortex solitons do not exist without the quintic term in the nonlinearity. Two types of the solitons, *viz.*, intersite- and onsite-centered ones (IC and OC, respectively), with even and odd numbers N of actually excited sites in the discrete direction, are identified. We consider the modes carrying the embedded vorticity $S = 1$ and 2 . In accordance with their symmetry, the vortex solitons of the OC type exhibit an intrinsic core, while the IC solitons with small N may have a coreless structure. Facilitating their creation in the experiment, the modes reported in the present work may be much more compact states than their counterparts considered in other systems, and they feature strong anisotropy. They can be set in motion in the discrete direction, provided that the coupling constant exceeds a certain minimum value. Collisions between moving vortex solitons are considered too.

Key words: Semidiscrete vortex soliton, cubic-quintic nonlinearity, intersite-centered, onsite-centered.

I. INTRODUCTION

The creation of stable solitons in multidimensional geometry is a subject of intensive ongoing research in nonlinear optics, Bose-Einstein condensates (BECs), and other fields [1, 2]. A fundamental problem which impedes straightforward making of such solitons is that the ubiquitous cubic self-focusing nonlinearity gives rise to the critical and supercritical collapse in the two- and three-dimensional (2D and 3D) space, respectively [3, 4], which destabilizes the solitons, on the contrary to stable ones supported by the cubic nonlinearity in 1D.

Thus, stabilization of multidimensional solitons is the central problem in this field. One possibility is the use of spatially periodic potentials, induced by photonic crystals in optics [5–7] and by optical lattices in BEC [8, 9]. In the limit of very deep periodic potentials, the nonlinear medium creates effectively discrete solitons [10–15]. Recently, another stabilization method was elaborated for two-component solitons, based on the use of the linear spin-orbit coupling in binary BEC [16–18], or its counterpart in the bimodal light propagation in planar waveguides [19].

STOP
The above-mentioned stabilization mechanisms for 2D and 3D solitons rely on the use of linear effects. The stability may also be provided by replacement of the cubic nonlinearity by other terms, which do not lead to the collapse. In optics, stable 2D spatial solitons and spatiotemporal light bullets were created in quadratic nonlinear crystals [20, 21], saturable [22] and nonlocal [23] nonlinear media, and, finally, in a bulk material which features competing cubic and quintic (CQ) focusing and defocusing interactions [24]. It is relevant to mention that the CQ nonlinearity, with negligible corrections from higher-order terms, was experimentally identified in optical materials such as CS₂ (for power densities up to hundreds of GW/cm² [25]) and colloidal suspensions of metallic nanoparticles [26, 27]. In BEC, stable 2D matter-wave solitons were predicted in dipolar BECs [28, 29] and microwave-coupled binary condensates [30], where the nonlinearity is cubic but effectively nonlocal. Recently, experiments have revealed soliton-like multidimensional matter-wave states, in the form of *quantum droplets* (QDs), filled by an incompressible ultradilute quantum fluid [31], in dipolar BECs [32–34], and in binary condensates with contact interactions [35–39]. The latter experiments followed the prediction of the stabilization of the QDs by the Lee-Huang-Yang (LHY) correction to the mean-field interactions [40], reported in Refs. [41, 42]. The correction originates from quantum fluctuations around the mean-field states.

*Electronic address: yongyaoli@gmail.com

A still more challenging issue is the creation of stable 2D and 3D bright solitons with embedded vorticity, because such a state is subject to the instability against splitting into fragments by azimuthal perturbations, which is a more destructive factor (the one acting faster) than the collapse [2]. Similar to their fundamental (zero-vorticity) counterparts, bright vortex solitons can be stabilized by means of linear effects, such as lattice potentials [8, 9, 43], and with the help of modified nonlinearity. In particular, effectively two-dimensional stable discrete and lattice optical vortex solitons were predicted [10] and created in the experiment [11–13]. Stable 2D solitons with intrinsic vorticity (topological charge) $S = 1$ in the uniform CQ medium were first predicted in Ref. [44], which was then extended to $S \geq 2$ [45, 46], and later to nonlinear lattices of the CQ type [47]. The existence of stable 3D solitons with $S = 1$ in the same model was reported in Ref. [48]. In binary BECs, stable 2D vortex solitons with topological charges up to $S = 5$ have been predicted in the above-mentioned microwave-coupled condensates, as well as in QDs with embedded vorticity [49, 50]. Stable 3D QDs filled by the “swirling” condensate with $S = 1$ and 2 were also revealed by the analysis [51].

A relevant extension of the analysis of topological solitons aims to predict stable vortex modes with an anisotropic shape. In optics, stable 2D discrete vortex states were predicted in 2D anisotropic discrete lattices [52, 54]. In BEC, vortex solitons were predicted in anisotropic lattice potentials [53], as well as in one component of the spin-orbit-coupled binary BEC with the anisotropic dipole-dipole interaction between atoms [55–57]. Very recently, creation of a novel form of 2D anisotropic vortices, *viz.*, *semidiscrete* QDs with imprinted vorticity, was elaborated in a system with one continuous and one discrete coordinates, realized as a binary condensate loaded in an array of parallel tunnel-coupled quasi-1D traps [58]. In that model, the intrinsic nonlinearity of the traps is represented by the combination of self-attractive quadratic LHY and repulsive cubic mean-field terms. A nontrivial peculiarity of the setting is identification of the vorticity, which is defined in terms of the global phase pattern carried by the semidiscrete state.

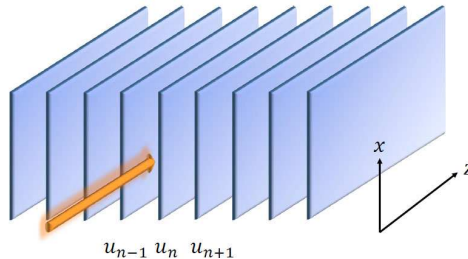


FIG. 1: The setting based on the array of planar optical waveguides (blue slabs), separated by gray isolating layers, with the continuous transverse coordinate, x , and the discrete one, n . As shown by the arrow, light is coupled into the array along the z direction.

Semidiscrete vortices were not yet considered in nonlinear optics, which is the subject of the present work. Because arrays of coupled nonlinear waveguides are ubiquitous systems in optics [14, 15], the creation of nontrivial self-trapped states in the arrays is a very relevant objective. The present work aims to predict stable semidiscrete optical vortex solitons in a effectively 2D setting built as an array of parallel tunnel-coupled planar waveguides with the intrinsic CQ nonlinearity, as sketched in Fig. 1. This setting may be naturally considered as a semidiscrete one. The respective model is somewhat similar to the above-mentioned one developed for the array of BEC traps with the intrinsic quadratic-cubic nonlinearity, which also supports stable vortex solitons [58]. However, results concerning the shape and stability of semidiscrete vortex solitons in the present system are essentially different. In particular, they may feature strong anisotropy, unlike quasi-isotropic modes reported in Ref. [58], and they may be built with much tighter shapes.

The rest of the paper is structured as follows. The model is introduced in Sec. II, including two possible realizations in optics, *viz.*, in terms of the light propagation in the spatial domain, as outlined in Fig. 1, and in the spatiotemporal one, realized as an array of tunnel-coupled fiber-like waveguides. Systematic results for the existence and stability of vortex solitons with $S = 1$ and $S = 2$ are summarized in Sec. III. The paper is concluded by Sec. IV.

II. THE MODEL

The propagation of light in the waveguiding array displayed in Fig. 1 is modeled, in the paraxial approximation, by coupled nonlinear Schrödinger equations (NLSEs) [59, 60] with the CQ terms [61]:

$$\begin{aligned} 2ik_0 \frac{\partial}{\partial Z} A_n &= -\frac{\partial^2}{\partial X^2} A_n - \kappa (A_{n+1} - 2A_n + A_{n-1}) \\ -2k_0^2 \frac{n_2}{n_0} |A_n|^2 A_n + 2k_0^2 \frac{n_4}{n_0} |A_n|^4 A_n - i\zeta A_n. \end{aligned} \quad (1)$$

where A_n is the envelope of the electromagnetic field in the n -th guiding core, with carrier wavenumber $k_0 = 2n_0\pi/\lambda$, κ is the strength of the tunnel coupling between adjacent cores, n_0 , n_2 and n_4 represent, respectively, the linear, third- and fifth-order refractive indices of the medium, and ζ is the loss coefficient. Equation (1) does not include multiphoton absorption (nonlinear losses), as we do not consider media with resonant interactions or ionization of the optical material, which would induce such losses [62]. The coupling constant is determined by the difference of the refractive index between the guiding cores and dielectric material which separates them, the carrier wavelength, and the thickness of the separating layer, exponentially decaying with the increase of the latter. In practical terms, experimentally relevant values of the thickness are tantamount to a few wavelengths (which corresponds to several microns). This choice leads to the propagation length, for which the coupling effects become essential, measured in several millimeters [14]. As concerns the losses, in available optical materials they take values \sim dB/m or still smaller, which makes the losses negligible for experimentally available propagation lengths $\lesssim 10$ cm. For this reason, the dissipative term is neglected in the following consideration.

The semidiscrete systems adequately modeled by Eq. (1) with the cubic-only nonlinearity ($n_4 = 0$), were first introduced, and soliton-like states in them were investigated, in Refs. [59, 63–67], in terms of the spatiotemporal propagation of light in arrays of optical fibers. On the other hand, the 2D discrete model with the CQ onsite nonlinearity, and discrete soliton modes in them, were considered in Ref. [68]. A 2D quasi-discrete model, combining a deep checkerboard potential and the CQ nonlinearity, was also addressed, along with its vortex-soliton modes, in Ref. [69].

By applying rescaling,

$$\begin{aligned} U_n &= \sqrt{n_4/n_2} A_n, \quad C = (n_0 n_4 / 2k_0^2 n_2^2) \kappa \\ z &= (k_0^2 n_2^2 / n_0 n_4) Z, \quad x = X k_0 n_2 / \sqrt{n_0 n_4}, \end{aligned} \quad (2)$$

Eq. (1) is cast in the normalized form,

$$\begin{aligned} i\partial_z U_n &= -\frac{1}{2} \partial_{xx} U_n - \frac{C}{2} (U_{n+1} - 2U_n + U_{n-1}) \\ &\quad - |U_n|^2 U_n + |U_n|^4 U_n, \end{aligned} \quad (3)$$

with the effective intersite coupling constant, C . The total power of the field in the scaled form, which is a dynamical invariant of Eq. (3), is defined as

$$P = \sum_{n=-\infty}^{+\infty} \int_{-\infty}^{+\infty} |U_n(x)|^2 dx. \quad (4)$$

The model also conserves the Hamiltonian,

$$H = \frac{1}{2} \sum_{n=-\infty}^{+\infty} \int_{-\infty}^{+\infty} \left[|\partial_x U_n|^2 + C |U_n - U_{n-1}|^2 - |U_n|^4 + \frac{2}{3} |U_n|^6 \right] dx. \quad (5)$$

To estimate physical parameters of the model, we assume that, for instance, the cubic-quintic material is CS_2 , which was used for the creation of stable fundamental 2D solitons in Ref. [24]. At the carrier wavelength $\lambda = 800$ nm, its parameters are $n_0 = 1.61$, $n_2 = 3.1 \times 10^{-19} \text{ m}^2/\text{W}$, and $n_4 = 5.2 \times 10^{-35} \text{ m}^4/\text{W}^2$ [70, 71]. Then, relations between scaled units in Eq. (3) and physical ones are estimated, by means of Eq. (2), as follows: $x = 1 \iff 0.235 \text{ } \mu\text{m}$, $z = 1 \iff 0.07 \text{ mm}$, and $P = 1 \iff 70 \text{ kW}$, if the thickness of the single planar waveguide is $0.5 \text{ } \mu\text{m}$. As mentioned above, the losses in the medium may be neglected for experimentally relevant propagation distances [24]. With respect to these estimates, the characteristic transverse size of self-trapped modes considered below, $\Delta x \sim 20 - 40$, corresponds to the physical width $\sim 5 - 10 \text{ } \mu\text{m}$, and the characteristic propagation distance, which is $z \sim 500 - 3000$,

amounts to $3.5 \sim 20$ cm. These values are realistic for feasible experiments, see Refs. [11–14]. Note also that Δx is sufficiently large in comparison to λ , which justifies the use of the paraxial propagation equation (3).

The same model applies to the temporal-domain light propagation, with carrier group velocity V_{gr} , in an array of tunnel-coupled optical fibers with the intrinsic CQ nonlinearity, if coordinate x in Eq. (3) is replaced by the temporal coordinate, $\tau = t - z/V_{\text{gr}}$. In that case, the solitons represent semidiscrete “light bullets”, and Eq. (4) defines the total energy of the spatiotemporal optical signal.

III. RESULTS

A. Semidiscrete vortex solitons with topological charge $S = 1$

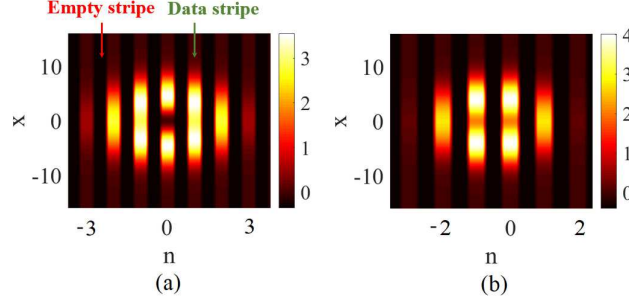


FIG. 2: Typical examples of the inputs used for the generation of vortex solitons of the OC (a) and IC (b) types, taken as per Eqs. (7) and, respectively, (8) or (9). Input (a) with parameters $(A, \alpha, P) = (0.85, 0.0015, 50)$ produces the OC soliton shown in Fig. 3(f). Input (b) with parameters $(A, \alpha, P) = (0.09, 0.0015, 40)$ produces the IC soliton shown in Fig. 3(b).

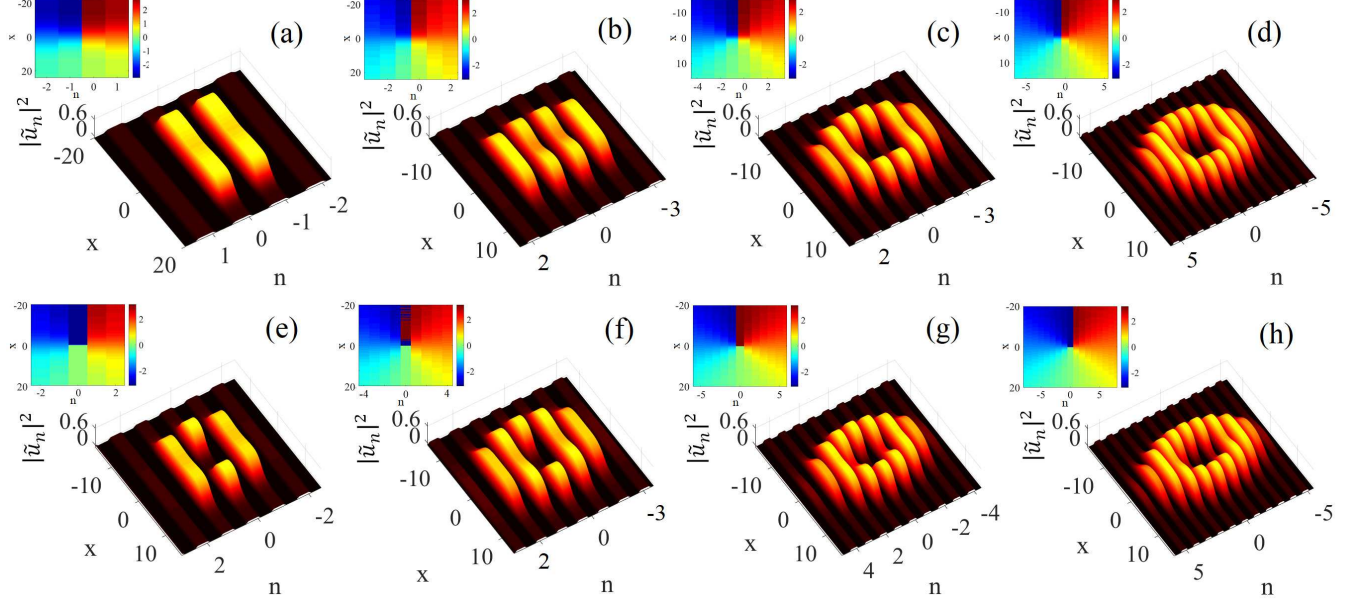


FIG. 3: (a-d) Typical examples of the intensity pattern of stable IC vortex solitons with $S = 1$, which correspond to points “A-D” in the stability areas in Fig. 4(a). Their parameters are $(P, C, N, N_{\text{core}}) = (39, 0.01, 2, 0)$ (a), $(40, 0.05, 4, 0)$ (b), $(55, 0.13, 6, 2)$ (c), and $(70, 0.21, 8, 2)$ (d). (e-f) Typical examples of the intensity pattern for stable OC vortex solitons with $S = 1$, which correspond to points “E-H” in the stability areas in Fig. 4(b). The corresponding parameters are $(P, C, N, N_{\text{core}}) = (32, 0.035, 3, 1)$ (e), $(50, 0.1, 5, 1)$ (f), $(65, 0.18, 7, 3)$ (g), and $(80, 0.27, 9, 3)$ (h). Insets display the respective phase patterns, which identify the soliton’s vorticity, $S = 1$.

Stationary solutions to Eq. (3) with propagation constant β are looked for as

$$U_n(x, z) = u_n(x)e^{i\beta z}. \quad (6)$$

Stationary semidiscrete vortex solitons with topological charge S , of the onsite-centered (OC) and intersite-centered (IC) types, with the pivot located, respectively, at a lattice site or between two sites, were produced by means of the power-conserving squared-operator numerical method [72], initiated by inputs

$$\phi_0 = AR^S \exp(iS\Theta - \alpha R^2), \quad (7)$$

where A and α are positive real constants. For the OC and IC solitons, we set in Eq. (7)

$$R_{\text{OC}}^2 = x^2 + (n/\sqrt{C})^2, \Theta_{\text{OC}} = \arctan(n/\sqrt{C}x), \quad (8)$$

$$R_{\text{IC}}^2 = x^2 + [(n + 1/2)/\sqrt{C}]^2, \Theta_{\text{IC}} = \arctan[(n + 1/2)/\sqrt{C}x], \quad (9)$$

respectively.

Examples of the inputs used for the generation of the OC and IC solitons are displayed in Fig. 2. To make the pictures clearer, in this and other figures values of local intensities, $|U_n(x)|^2$, are shown, at discrete values of n , by means of finite-width stripes separated by empty ones [“data” and “empty” stripes in Fig. 2(a)].

Then, stability of the stationary solutions was verified by direct simulations of Eq. (3) for propagation distance $z = 1000$. The soliton is stable if its intensity profile stays unchanged throughout the simulation. According to the above-mentioned estimate of parameters for CS_2 , $z = 1000$ corresponds to $Z = 7$ cm, which is sufficiently long for observing a stable spatial soliton in the experiment. In the numerical computations, control parameters are total power P (4) and coupling constant C in Eq. (3). In terms of vortex modes displayed below in Fig. 3, $z = 1000$ corresponds to $\gtrsim 10$ characteristic Rayleigh (diffraction) lengths with respect to the continuous and discrete coordinates, hence this distance is sufficient to make conclusions concerning the stability of the modes.

Typical examples of the vortex solitons of the OC and IC types are displayed in Fig. 3 [the sign of the vorticity, $S = 1$, is determined by the comparison of phase patterns in the figure with the standard expression, $u \sim \exp(iS\Theta)$, in the continuum coordinate plane with angular coordinate Θ]. The solitons are characterized by the number of effectively excited sites, N (individual waveguides in which the field takes non-negligible values). Another important characteristic is number N_{core} of sites in the *core* of the semidiscrete vortex, i.e., waveguides in which stationary fields $u_n(x)$ [see Eq. (6)] cross zero (vanish) at $x = 0$, thus having opposite signs at $x > 0$ and $x < 0$, while zero crossing is absent in waveguides which do not belong to the core. Although fundamental semidiscrete solitons, with zero vorticity, are also characterized by finite N [59, 63–67], only vortices may feature the core. Examples displayed in Fig. 3 exhibit values of the excited and in-core sites $2 \leq N \leq 9$ and $0 \leq N_{\text{core}} \leq 3$, with odd and even numbers N and N_{core} pertaining, severally, to the vortex modes of the OC and IC types. Note that the states of the former type always have $N_{\text{core}} \geq 1$, and, due to their intrinsic symmetry, any vortex soliton of the OC type with odd S has a real odd modal function $u_0(x)$ in the central waveguide ($n = 0$), see Fig. 5(a) below. On the other hand, the IC vortex states may exist both with $N_{\text{core}} = 0$ and $N_{\text{core}} \geq 2$, see panels (a,b) and (c,d) in Fig. 3. In the case of $N_{\text{core}} = 0$, the vorticity is accounted for by opposite signs of fields $u_0(x)$ and $u_1(x)$ in Eq. (6), with the “virtual pivot” of the vortex set between $n = 0$ and $n = 1$. It is also worthy to note that the semidiscrete vortex solitons may be strongly anisotropic, elongated in the continuous direction, in the case of small C , see, e.g., Figs. 3(a,e). On the other hand, Fig. 6, displayed below, demonstrates that stable vortices slightly elongated in the discrete direction, exist too, corresponding to $\varepsilon < 1$ in Fig. 6.

Stability areas for the OC and IC species of semidiscrete vortex solitons, which are characterized by numbers N , are displayed in the (P, C) plane in Figs. 4(a,b). A remarkable feature of the stability chart is *bistability*, allowing coexistence of the vortices with equal powers P and different numbers of sites, and even *tristability* – in particular, the overlap of the stability regions for the vortices of the IC type with $N = 4, 6, 8$, at $P > 83$ [see point X in Fig. 4(a)]. In fact, the multistability area is even broader, as Fig. 4(b) demonstrates that, in addition to these three IC modes, two stable vortices of the OC type exist too, with $N = 5$ and 7 , at the same values of C and P . In the limit of $P \rightarrow \infty$, which corresponds to the 2D continuum space, the multistability agrees with the known fact that 2D vortex solitons of the nonlinear Schrödinger equation with CQ nonlinearities become stable as the solitons expand to accommodate indefinitely growing values of the norm [45]. The calculation of values of the Hamiltonian, according to Eq. (5), demonstrates that the minimum of the Hamiltonian, i.e., the ground state of the system, is realized, in the case of bi- or tristability, by the mode with the smallest number of excited discrete sites. An example of this calculation is shown in Fig. 4(c,d). Typically, the tristability area for the IC solitons with $N = 4, 6$ and 8 is shaded in Fig. 4(c). Recently, multistability has also been found in 1D quantum droplets trapped in a lattice potential [73].

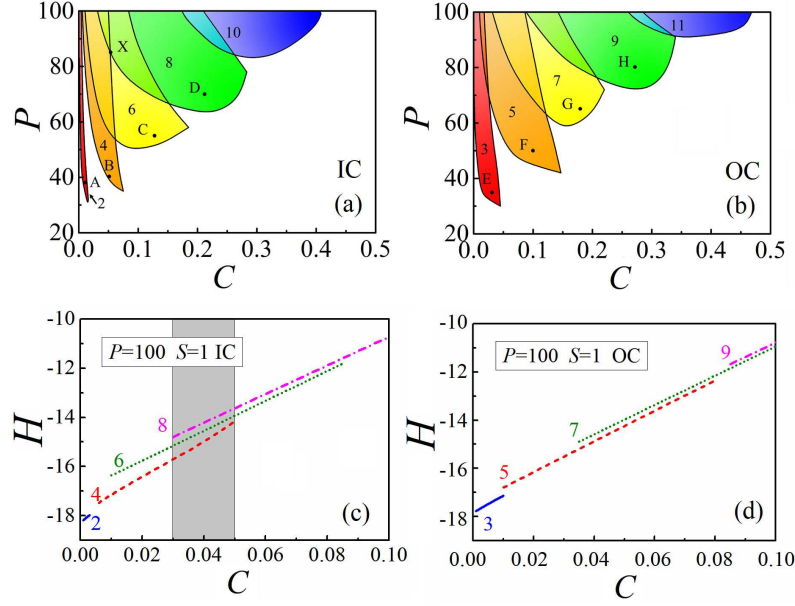


FIG. 4: (Color online) Stability areas for semidiscrete vortex solitons of the IC (a) and OC (b) types, in the (P, C) plane (the total power and intersite coupling constant). Vortex-soliton species are characterized by the number of excited sites, N , and the size of the vortex's core, N_{core} , in the discrete direction. These numbers, which are even in (a) and odd in (b), label particular colored stability regions. (c,d) H as a function of C at $P = 100$ for stable vortex solitons of the IC and OC type with different values of N and N_{core} . The tristability for a given value of P occurs in the gray stripe in panel (c), where, obviously, the vortex mode with the smallest values of N and N_{core} realizes the system's ground state.

Outside of the stability area but close to its border, unstable vortex solitons can also be found; in direct simulations, they split in fragments. Typical examples of the evolution of stable and unstable vortex solitons are displayed in Fig. 5. Far from the stability boundary of the vortices, only fundamental (zero-vorticity) solitons are produced by the numerical calculations.

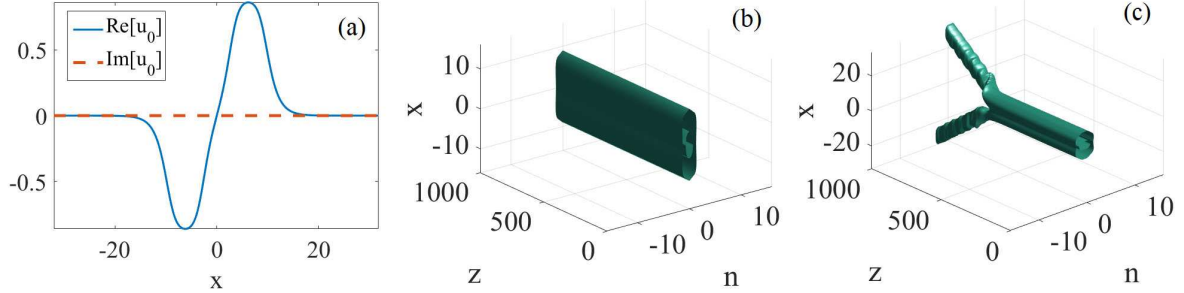


FIG. 5: (a) Real and imaginary parts of the stationary wave function of the OC soliton from Fig. 3(e) in the central ($n = 0$) waveguide. As explained in the text, the stationary wave field at the center of OC vortex solitons with $S = 1$ is real and spatially odd. (b) Direct simulations of the perturbed evolution of a stable OC soliton with $(P, C, N, N_{\text{core}}) = (32, 0.035, 3, 1)$. (c) Direct simulations for an unstable OC soliton with $(P, C, N, N_{\text{core}}) = (33, 0.07, 3, 1)$.

Note that the vortex solitons of the IC and OC types with only two and three excited sites (and, respectively, $N_{\text{core}} = 0$ and $N_{\text{core}} = 1$) realize two types of the solitons with the minimum size in the discrete direction. Such tightly localized semidiscrete modes were not reported in the previously studied semidiscrete system [58]. In fully discrete 2D models, the possibility that the smallest vortex soliton includes four sites was theoretically predicted [10] and experimentally demonstrated [12, 13].

Figure 6(a) displays the propagation constant, β , for two types of compact solitons [IC and OC with $(N, N_{\text{core}}) = (4, 0)$ and $(N, N_{\text{core}}) = (5, 1)$, respectively] as a function of the total power, P , for fixed C . These results indicate that the $\beta(P)$ curves satisfy the Vakhitov-Kolokolov criterion, $d\beta/dP > 0$, which is a well-known necessary stability condition [3, 74]. Figure 6(b) shows the $\beta(C)$ dependence for stable vortex solitons with different numbers of excited

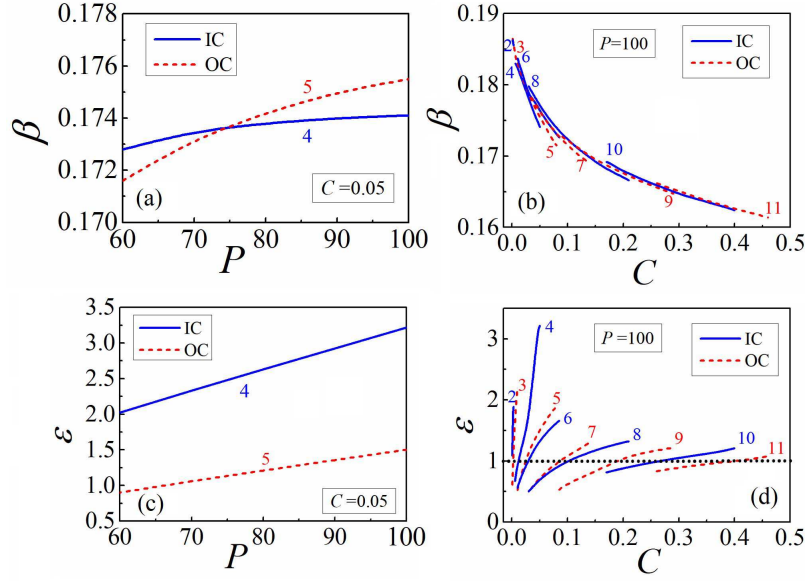


FIG. 6: (a) Propagation constant β [see Eq. (6)] vs. the total power, P , for families of stable solitons of the IC and OC types, which contain $N = 4$ or 5 excited sites in the discrete direction, respectively, for $C = 0.05$. The corresponding values of the core's size are $N_{\text{core}} = 0$ and 1 . (b) β vs. the coupling constant, C , for the families of stable solitons with different numbers of N and N_{core} . Here, we fix $P = 100$. (c) The anisotropy measure ε , defined as per Eq. (10) for the vortex solitons, with $(N, N_{\text{core}}) = (4, 0)$ and $(N, N_{\text{core}}) = (5, 1)$, vs. P , for $C = 0.05$. (d) ε for the stable vortex states, with different values of N and N_{core} , as a function of C , for fixed $P = 100$. Extensions of the displayed branches (which are not shown in the figure) are formed by unstable solitons.

sites N and fixed P , showing that β gradually decreases with C .

To characterize anisotropy of the vortex soliton, we define parameter

$$\varepsilon = \sqrt{C} \frac{L_x}{L_n}, \quad (10)$$

$$L_x \equiv \frac{\left(\int_{-\infty}^{+\infty} |u_0(x)|^2 dx \right)^2}{\int_{-\infty}^{+\infty} |u_0(x)|^4 dx}, \quad L_n \equiv \frac{(\sum_n |u_n(x=0)|^2)^2}{\sum_n |u_n(x=0)|^4}. \quad (11)$$

This definition is adopted from Ref. [58], where $\varepsilon = 1$ implied that solitons were effectively isotropic modes, while $\varepsilon > 1$ and $\varepsilon < 1$ indicated that their shape was anisotropic, namely, elongated in the continuous or discrete direction, respectively. Figure 6(c) displays ε as a function of P for the compact vortex solitons with $(N, N_{\text{core}}) = (4, 0)$ and $(N, N_{\text{core}}) = (5, 1)$. This figure indicates that ε grows, approximately, as a linear function of P . Figure 6(d) displays the $\varepsilon(C)$ curves for vortex solitons with different values of N and N_{core} , and fixed P . The figure shows that the slope of $\varepsilon(C)$ decreases with the increase of N . Naturally, values of $\varepsilon(C)$ get closer to the isotropy point, $\varepsilon = 1$, for larger N , as this case corresponds to the quasi-continuum limit of the system in the discrete direction, with the vortex soliton getting less compact. Moreover, passage of $\varepsilon(P)$ and $\varepsilon(C)$ through the level of $\varepsilon = 1$ implies that the vortex solitons may be tuned to the isotropic shape by selecting specific values of P or C .

B. Effect of the relative strengths of the cubic and quintic nonlinearities

A natural question is how the competing self-focusing cubic and defocusing quintic onsite terms in Eq. (3) affect the existence and stability of semidiscrete vortex solitons. To address this issue, we here rescale the equation, to make the intersite coupling constant equal to 1 and admit the presence of a free coefficient in front of the quintic term as a free parameter:

$$\tilde{U}_n = \sqrt{C} U_n, \tilde{z} = z/C, \tilde{x} = x/\sqrt{C}, \quad (12)$$

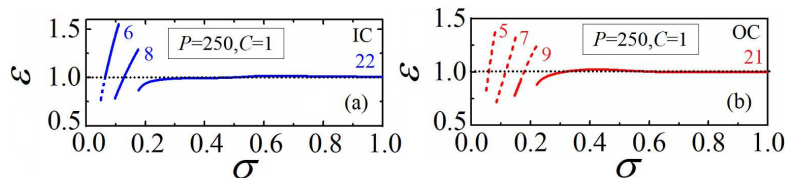


FIG. 7: Anisotropy parameter ε as a function of the relative strength of the quintic nonlinearity, σ , for semidiscrete vortex solitons with $S = 1$, of the IC (a) and OC (b) types, as produced by Eq. (13), with fixed total power $P = 250$. Solid and dashed curves represent stable and unstable solutions, respectively. Numbers attached to different segments denote the number N of excited sites in the respective semidiscrete modes [even values $8 < N < 22$ in (a), and odd ones $9 < N < 21$ in (b) show a gradual transition between the presented branches]. Long branches close to $\varepsilon = 1$ correspond to broad quasi-continuum modes with large values of N [in particular, with $N = 22$ and 21 , as indicated in panels (a) and (b)].

hence the rescaled total norm is $\tilde{P} = \sqrt{C}P$. The substitution of rescaling (12) in Eq. (3) casts it in the following form, where we omit the tilde, and use symbol $\sigma \equiv C$, to stress that C appears here as a newly defined parameter controlling the relative strength of the quintic term:

$$i\partial_z \tilde{U}_n = -\frac{1}{2}\partial_{\tilde{x}\tilde{x}} \tilde{U}_n - \frac{1}{2}(\tilde{U}_{n+1} - 2\tilde{U}_n + \tilde{U}_{n-1}) - |\tilde{U}_n|^2 \tilde{U}_n + \sigma |\tilde{U}_n|^4 \tilde{U}_n. \quad (13)$$

To characterize effects of the competition between the cubic and quintic nonlinearities, Fig. 7 displays anisotropy parameter ε [see Eq. (10)] as a function of σ for the IC and OC vortex solitons, as obtained from the numerical solution of Eq. (13) with a fixed total power, $P = 250$. The figure shows that, at $\sigma > 0.2$, ε stays very close to $\varepsilon = 1$, which indicates that the semidiscrete vortex solitons keep an effectively isotropic profile (hence, they have a broad quasi-continuum shape) in this case. At $\sigma < 0.2$, the vortex solitons feature a compact shape, adequately characterized by the number of excited sites, N . The segments, which are characterized by the number of excited sites $5 \leq N \leq 9$, terminate in Figs. 7(a,b) at their top and bottom points because solutions could not be found above or below them. At still smaller values of σ the vortex solitons are unstable, and no vortex modes were found at $\sigma \rightarrow 0$, when the CQ nonlinearity turn into the cubic form. Thus, the inclusion of the self-defocusing quintic term is *necessary* for the existence and stability of the semidiscrete vortex solitons.

C. Vortex solitons with $S = 2$

A challenging issue is whether stable vortex solitons can be found for the double topological charge, $S = 2$. Numerical results demonstrate that such solitons indeed exist – naturally, with larger powers than their counterparts with $S = 1$. They can be found, at least, at $P > 200$. Here, we fix $P = 250$ and consider characteristics of the vortex solitons with $S = 2$, varying intersite coupling C . The minimum numbers of sites necessary for constructing the double-vortex modes of the IC and OC types are $N = 6$ (with $N_{\text{core}} = 2$) and $N = 7$ (with $N_{\text{core}} = 3$), respectively. Typical examples for $6 \leq N \leq 13$ and $2 \leq N_{\text{core}} \leq 5$ (even and odd N and N_{core} for the solitons of the IC and OC types, respectively) are displayed in Fig. 8, and dependences $\beta(C)$ and $\varepsilon(C)$ for stable vortex solitons with $S = 2$ and different values of N are displayed in Fig. 9.

The intrinsic symmetry of the vortex solitons of the OC type, with even vorticity $S \geq 2$, predicts that its modal wave function in the central waveguide ($n = 0$), $u_0(x)$, is a real even function vanishing at $x = 0$. Indeed, an example displayed in Fig. 10(a) clearly corroborates the prediction. This feature may be compared to its counterpart in the case of $S = 1$, i.e., the odd real wave function $u_0(x)$, see Fig. 5(a) above. It is also worthy to stress that, while $u_0(x)$ virtually vanishes in a broad core area in Fig. 10(a), $u_0(x)$ keeps small positive values at all $x \neq 0$, i.e., it does not cross zero.

Similar to what is demonstrated above for $S = 1$, Fig. 9(a) shows that β gradually decreases with the increase of C , while $\varepsilon(C)$ may strongly deviate from $\varepsilon = 1$, indicating strong anisotropy of vortex solitons with $S = 2$ [see in Fig. 9(b)]. The branches shown in Fig. 8 are completely stable, whereas their extensions, not shown in the figure, carry solitons which are unstable against splitting in the discrete direction. Typical examples of the evolution of the stable and unstable vortex solitons with $S = 2$ are displayed in Figs. 10(b,c). A comparison of values of the Hamiltonian between the vortex solitons with $S = 1$ and 2 , which have equal powers, P , are shown in Figs. 9(c,d). The comparison indicates that, for the same N , the Hamiltonian is smaller for $S = 1$. Furthermore, the existence region for the vortices with $S = 1$ is larger (in some cases, much larger) than that for their counterparts with $S = 2$.

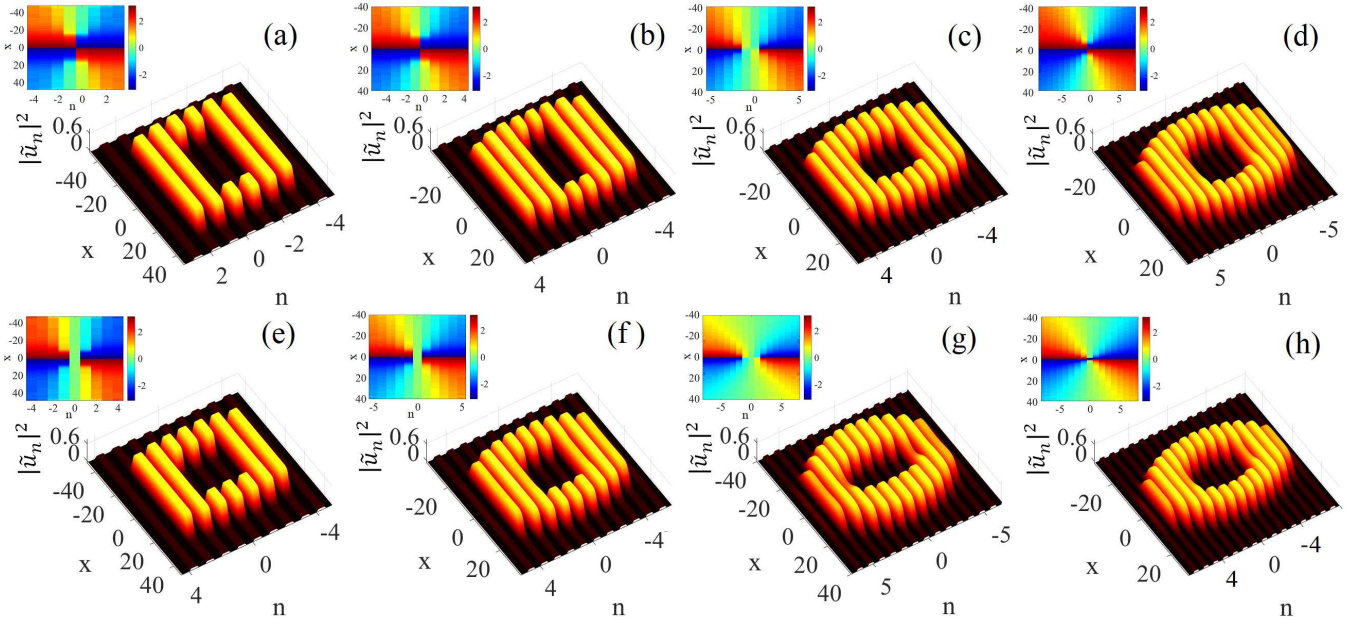


FIG. 8: (a-d) Typical examples of the intensity pattern for stable IC vortex solitons with $S = 2$, for parameters $(P, C, N, N_{\text{core}}) = (250, 0.01, 6, 2)$ (a), $(250, 0.03, 8, 2)$ (b), $(250, 0.04, 10, 4)$ (c), and $(250, 0.1, 12, 4)$ (d). (e-f) The same for stable vortex solitons with $S = 2$ of the OC type, with $(P, C, N, N_{\text{core}}) = (250, 0.01, 7, 3)$ (e), $(250, 0.04, 9, 3)$ (f), $(250, 0.1, 11, 5)$ (g), and $(250, 0.12, 13, 5)$ (h). Insets display the respective phase patterns, which identify the vorticity, $S = 2$.

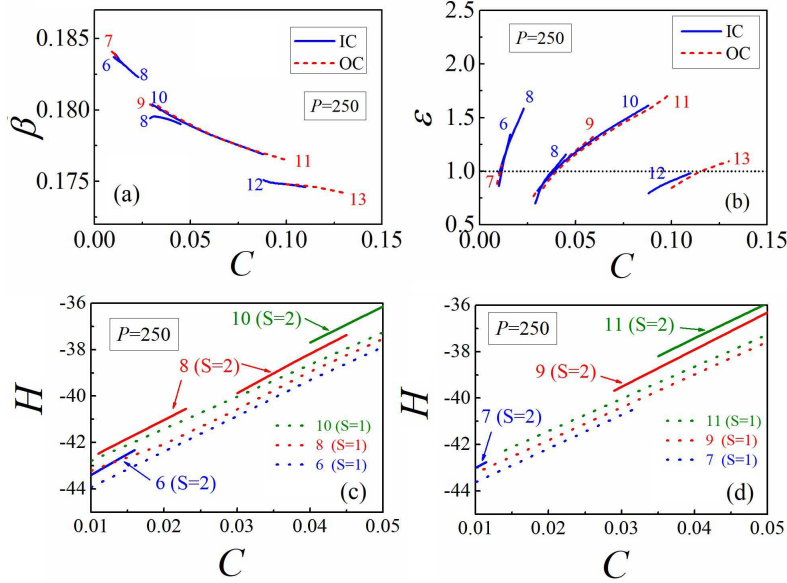


FIG. 9: (a) Dependences $\beta(C)$ for stable vortex solitons with $S = 2$, fixed total power, $P = 250$, and different numbers N of excited sites (extensions of the branches, which are not shown here, are formed by unstable solitons). (b) The same as in (a) but showing $\varepsilon(C)$ dependences for stable vortex solitons with $S = 2$. (c,d) The comparison of values of the Hamiltonian of the vortex solitons with $S = 1$ and 2 (dotted and solid segments, respectively), and equal total powers, $P = 250$, of the IC (c) and OC (d) types.

Interestingly, two different stable branches are found for $N = 8$ with smaller and larger values of C , which are shown by the two red-color segments in Fig. 9(c). This result implies that there are two types of vortex soliton with $S = 2$ for $N = 8$. To illustrate this conclusion, Fig. 8(b) shows an example of the vortex state belonging to the branch with larger C and $N_{\text{core}} = 2$. An example of the stable vortex soliton from the branch with smaller C is displayed in

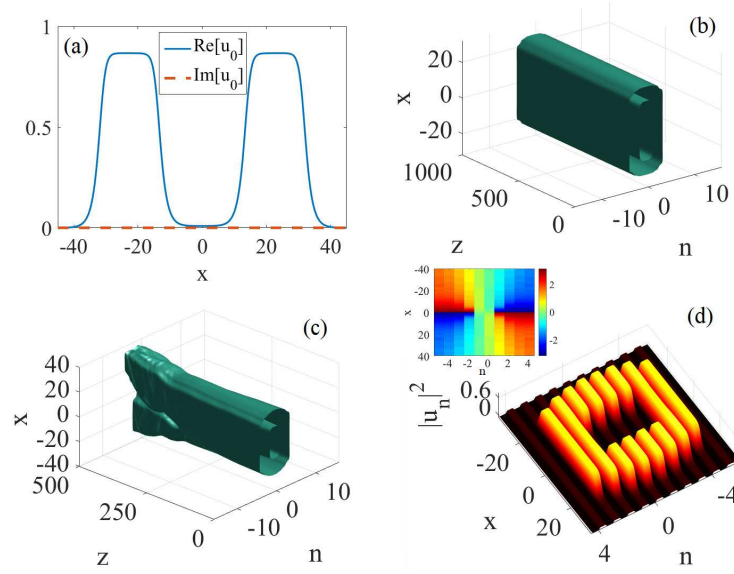


FIG. 10: (a) Real and imaginary parts of the OC soliton from Fig. 8(e) in the central waveguide, $n = 0$. (b) Direct simulations of the perturbed evolution of a stable vortex soliton of the IC type, with $S = 2$ and $(P, C, N, N_{\text{core}}) = (250, 0.03, 8, 2)$. (c) The perturbed evolution of an unstable soliton of the same type, with $(P, C, N, N_{\text{core}}) = (250, 0.25, 8, 2)$. (d) A typical example of stable IC vortex solitons with double vorticity, $S = 2$, the parameters being $(P, C, N, N_{\text{core}}) = (250, 0.018, 8, 4)$. The subplot is the respective phase pattern, which identifies the vorticity, $S = 2$. In comparison to its counterpart displayed in Fig. 8(b), this soliton represents the branch corresponding to smaller values of C , see further details in the text.

Fig. 10(d), with $N_{\text{core}} = 4$.

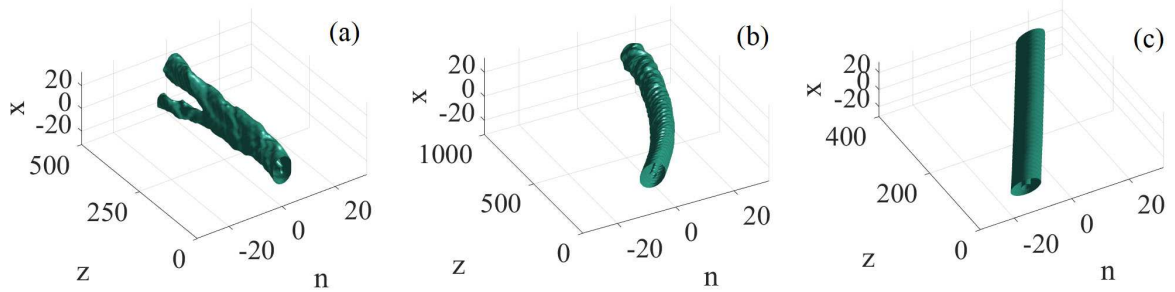


FIG. 11: (a) The vortex soliton with $(P, C) = (100, 0.1)$, destroyed by the application of the kick, as per Eq. (14). (b) A finite jump of the kicked vortex soliton, with $(P, C) = (100, 0.18)$. (c) An example of a mobile vortex soliton, with $(P, C) = (100, 0.3)$. The strength of the kick in all cases is $\eta = 0.1\pi$.

D. Mobility of the semidiscrete vortex solitons

A nontrivial issue is mobility of the vortex solitons in the discrete direction, initialized by the application of a kick, with strength η , to them:

$$U_n(x, z = 0) = U_n^{(0)}(x)e^{i\eta n}, \quad (14)$$

where $U_n^{(0)}(x)$ represents a quiescent soliton. Here, we address this issue for $U_n^{(0)}(x)$ taken as the stable vortex of the OC type with $S = 1$ and $P = 100$. At $C < 0.2$, the kick cannot set the soliton in progressive motion, just destroying it if η is too large, as shown in Fig. 11(a), or causing a finite leap, as shown in Fig. 11(b). The kicked vortex soliton demonstrates mobility at moderate discreteness, with $C > 0.2$, see an example in Fig. 11(c).

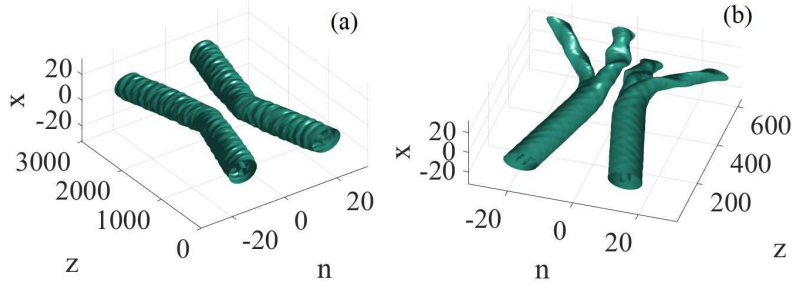


FIG. 12: (a) Elastic collision between two moving semidiscrete vortex solitons, kicked by $\eta = \pm 0.01\pi$. (b) Inelastic collision between moving solitons, kicked by $\eta = \pm 0.03\pi$. In the latter case, each vortex soliton splits in two fragments after the collision. Here, we select the vortex solitons with parameters $(P, C) = (100, 0.3)$, originally placed at positions $n_0 = \pm 16$.

Collisions between two vortex solitons moving in the opposite discrete directions can be initialized by taking

$$U_n(x, z = 0) = U_{+n_0}^{(0)}(x)e^{i\eta n} + U_{-n_0}^{(0)}(x)e^{-i\eta n}, \quad (15)$$

where $2n_0$ is the initial separation between the solitons. Elastic collisions occur if η is small. In this case, the two colliding vortex solitons retain their vorticities after the collision. Inelastic collisions occur between the vortex solitons kicked with larger values of η . In this case, the collision splits each soliton in fragments. Figure 12 shows typical examples of elastic and inelastic collisions for the vortex solitons with $(P, C, \pm n_0) = (100, 0.3, \pm 16)$. In this case, the collision remains elastic at $\eta < 0.016\pi$.

IV. CONCLUSION

We have introduced the spatial-domain model for stacked set of tunnel-coupled planar waveguides with the combination of intrinsic self-focusing and defocusing cubic and quintic nonlinearities. The model applies as well to arrays of tunnel-coupled fiber waveguides with the same nonlinearity and anomalous group-velocity dispersion, which is a temporal-domain counterpart of the paraxial diffraction in planar guiding cores. Unlike fundamental semidiscrete solitons, previously studied in a similar model with the cubic-only nonlinearity, we here aimed to construct solitons with embedded vorticities, $S = 1$ and 2 . It is found that such vortex solitons of the IC and OC (intersite- and onsite-centered) types, composed of N excited sites carrying non-negligible amplitudes in the transverse direction, form stable families, starting from minimum values $(N_{IC})_{\min} = 2$ and $(N_{OC})_{\min} = 3$, respectively. The semidiscrete vortex solitons of the OC type always feature an internal core, while the IC solitons with small N may have a coreless structure. The system admits multistability, i.e., coexistence of stable vortex solitons with equal norms and different values of N . The existence and stability of such modes are only possible when the quintic defocusing term is not too small. The vortex solitons feature mobility in the discrete direction, provided that the coefficient of the intersite coupling exceeds a certain minimum value. Semidiscrete vortex solitons moving in opposite directions collide elastically or inelastically if they are set in motion by relatively weak or strong kicks, respectively.

Acknowledgments

This work was supported by the Key Research Projects of General Colleges in Guangdong Province through grant No. 2019KZDXM001, NNSFC (China) through grant Nos. 11905032, 11874112, and 11575063, the Foundation for Distinguished Young Talents in Higher Education of Guangdong through grant No. 2018KQNCX279. The work of B.A.M. is supported, in a part, by Israel Science Foundation through grant No. 1286/17.

-
- [1] Y. Kartashov, G. Astrakharchik, B. Malomed, and L. Torner, Frontiers in multidimensional self-trapping of nonlinear fields and matter, *Nature Reviews Physics* **1**, 185-197 (2019).
 - [2] B. A. Malomed, Vortex solitons: Old results and new perspectives, *Physica D* **399** 108 (2019).
 - [3] L. Bergé, Wave collapse in physics: Principles and applications to light and plasma waves, *Phys. Rep.* **303**, 259 (1998).

- [4] G. Fibich, *The Nonlinear Schrödinger Equation: Singular Solutions and Optical Collapse* (Springer, Heidelberg, 2015).
- [5] Y. S. Kivshar and G. P. Agrawal, *Optical Solitons: From Fibers to Photonic Crystals*, (Academic Press, San Diego, 2003).
- [6] M. Skorobogatiy and J. Yang, *Fundamentals of Photonic Crystal Guiding* (Cambridge University Press, Cambridge, 2009).
- [7] I. L. Garanovich, S. Longhi, A. A. Sukhorukov, Y. S. Kivshar, Light propagation and localization in modulated photonic lattices and waveguides, *Phys. Rep.* **518**, 1 (2012).
- [8] B. B. Baizakov, B. A. Malomed, and M. Salerno, Multidimensional solitons in periodic potentials, *Europhys. Lett.* **63**, 642-648 (2003).
- [9] J. Yang, Z. H. Musslimani, Fundamental and vortex solitons in a two-dimensional optical lattice, *Opt. Lett.* **28** 2094 (2003).
- [10] B. A. Malomed and P. G. Kevrekidis, Discrete vortex solitons, *Phys. Rev. E* **64**, 026601 (2001).
- [11] H. Martin, E. D. Eugenieva, Z. Chen, and D. N. Christodoulides, Discrete solitons and soliton-induced dislocations in partially coherent photonic lattices, *Phys. Rev. Lett.* **92**, 123902 (2004).
- [12] D. N. Neshev, T. J. Alexander, E. A. Ostrovskaya, Y. S. Kivshar, H. Martin, I. Makasyuk, and Z. Chen, Observation of discrete vortex solitons in optically induced photonic lattices, *Phys. Rev. Lett.* **92**, 123903 (2004).
- [13] J. W. Fleischer, G. Bartal, O. Cohen, O. Manela, M. Segev, J. Hudock, and D. N. Christodoulides, Observation of vortex-ring “discrete” solitons in 2D photonic lattices, *Phys. Rev. Lett.* **92** 123904 (2004).
- [14] F. Lederer, G. I. Stegeman, D. N. Christodoulides, G. Assanto, M. Segev, Y. Silberberg, Discrete solitons in optics, *Phys. Rep.* **463**, 1 (2008).
- [15] B. A. Malomed, Nonlinearity and discreteness: Solitons in lattices, in *Emerging Frontiers in Nonlinear Science*, pp. 81-110, ed. by P. G. Kevrekidis, J. Cuevas-Maraver, and A. Saxena (Springer Nature Switzerland AG: Cham, 2020).
- [16] H. Sakaguchi, B. A. Malomed, Creation of two-dimensional composite solitons in spin-orbit-coupled self-attractive Bose-Einstein condensates in free space, *Phys. Rev. E* **89**, 032920 (2014).
- [17] Y.-C. Zhang, Z.-W. Zhou, B. A. Malomed, and H. Pu, Stable solitons in three dimensional free space without the ground state: Self-trapped Bose-Einstein condensates with spin-orbit coupling, *Phys. Rev. Lett.* **115**, 253902 (2015).
- [18] B. A. Malomed, Creating solitons by means of spin-orbit coupling, *Europhys. Lett.* **122**, 36001 (2018).
- [19] Y. V. Kartashov, B. A. Malomed, V. V. Konotop, V. E. Lobanov, and L. Torner, Stabilization of spatiotemporal solitons in Kerr media by dispersive coupling, *Opt. Lett.* **40**, 1045 (2015).
- [20] W. E. Torruellas, Z. Wang, D. J. Hagan, E. W. VanStryland, G. I. Stegeman, L. Torner, and C. R. Menyuk, Observation of Two-Dimensional Spatial Solitary Waves in a Quadratic Medium, *Phys. Rev. Lett.* **74**, 5036 (1995).
- [21] X. Liu, K. Beckwitt, and F. Wise, Two-dimensional optical spatiotemporal solitons in quadratic media, *Phys. Rev. E* **62**, 1328 (2000).
- [22] M. Segev, G. C. Valley, B. Crosignani, P. DiPorto, and A. Yariv, Steady-State Spatial Screening Solitons in Photorefractive Materials with External Applied Field, *Phys. Rev. Lett.* **73**, 3211 (1994).
- [23] M. Pccianti, K. A. Brzdakiewicz, and G. Assanto, Nonlocal spatial soliton interactions in nematic liquid crystals, *Opt. Lett.* **27** 1460 (2002).
- [24] E. L. Falcão-Filho, C. B. de Araújo, G. Boudebs, H. Leblond, and V. Skarka, Robust two-dimensional spatial solitons in liquid carbon disulfide, *Phys. Rev. Lett.* **110**, 013901 (2013).
- [25] D. G. Kong, Q. Chang, H. Ye, Y. C. Gao, Y. X. Wang, X. R. Zhang, K. Yang, W. Z. Wu, and Y. L. Song, The fifth-order nonlinearity of CS₂, *J. Phys. B: At. Mol. Opt. Phys.* **42**, 065401 (2009).
- [26] A. S. Reyna and C. B. de Araújo, Nonlinearity management of photonic composites and observation of spatial-modulation instability due to quintic nonlinearity, *Phys. Rev. A* **89**, 063803 (2014).
- [27] A. S. Reyna and C. B. de Araújo, High-order optical nonlinearities in plasmonic nanocomposites – a review, *Adv. Opt. Phot.* **9**, 720-773 (2017).
- [28] P. Pedri and L. Santos, Two-Dimensional Bright Solitons in Dipolar Bose-Einstein Condensates, *Phys. Rev. Lett.* **95**, 200404 (2005).
- [29] I. Tikhonenkov, B. A. Malomed, and A. Vardi, Anisotropic Solitons in Dipolar Bose-Einstein Condensates, *Phys. Rev. Lett.* **100**, 090406 (2008).
- [30] J. Qin, G. Dong, and B. A. Malomed, Stable giant vortex annuli in microwave-coupled atomic condensates, *Phys. Rev. A* **94**, 053611 (2016).
- [31] Z. Luo, W. Pang, B. Liu, Y. Li, B. A. Malomed, A new form of liquid matter: Quantum droplets, *Front. Phys.* **16**, 32501 (2021).
- [32] M. Schmitt, M. Wenzel, F. Böttcher, I. Ferrier-Barbut, and T. Pfau, Self-bound droplets of a dilute magnetic quantum liquid, *Nature* **539**, 259 (2016).
- [33] D. Baillie, R. M. Wilson, R. N. Bisset, and P. B. Blakie, Self-bound dipolar droplet: A localized matter wave in free space, *Phys. Rev. A* **94**, 021602(R) (2016).
- [34] L. Chomaz, S. Baier, D. Petter, M. J. Mark, F. Wächtler, L. Santos, and F. Ferlaino, Quantum-Fluctuation-Driven Crossover from a Dilute Bose-Einstein Condensate to a Macrodroplet in a Dipolar Quantum Fluid, *Phys. Rev. X* **6**, 041039 (2016).
- [35] C. R. Cabrera, L. Tanzi, J. Sanz, B. Naylor, P. Thomas, P. Cheiney, and L. Tarruell, Quantum liquid droplets in a mixture of Bose-Einstein condensates, *Science* **359**, 301 (2018).
- [36] P. Cheiney, C. R. Cabrera, J. Sanz, B. Naylor, L. Tanzi, and L. Tarruell, Bright soliton to quantum droplet transition in a mixture of Bose-Einstein condensates, *Phys. Rev. Lett.* **120**, 135301 (2018).
- [37] G. Semeghini, G. Ferioli, L. Masi, C. Mazzinghi, L. Wolswijk, F. Minardi, M. Modugno, G. Modugno, M. Inguscio, and M. Fattori, Self-bound quantum droplets of atomic mixtures in free space, *Phys. Rev. Lett.* **120**, 235301 (2018).

- [38] G. Ferioli, G. Semeghini, L. Masi, G. Giusti, G. Modugno, M. Inguscio, A. Gallemi, A. Recati, and M. Fattori, Collisions of self-bound quantum droplets, *Phys. Rev. Lett.* **122**, 090401 (2019).
- [39] C. D'Errico, A. Burchianti, M. Prevedelli, L. Salasnich, F. Ancilotto, M. Modugno, F. Minardi, and C. Fort, Observation of quantum droplets in a heteronuclear bosonic mixture, *Phys. Rev. Research* **1**, 033155 (2019).
- [40] T. D. Lee, K. S. Huang, and C. N. Yang, Eigenvalues and eigenfunctions of a Bose system of hard spheres and Its Low-temperature properties, *Phys. Rev.* **106**, 1135 (1957).
- [41] D. S. Petrov, Quantum Mechanical Stabilization of a Collapsing Bose-Bose Mixture, *Phys. Rev. Lett.* **115**, 155302 (2015).
- [42] D. S. Petrov and G. E. Astrakharchik, Ultradilute Low-Dimensional Liquids, *Phys. Rev. Lett.* **117**, 100401 (2016).
- [43] Y. Zheng, S. Chen, Z. Huang, S. Dai, B. Liu, Y. Li, S. Wang, Quantum droplets in two-dimensional optical lattices, *Front. Phys.* **16**, 22501 (2021).
- [44] M. Quiroga-Teixeiro and H. Michinel, Stable azimuthal stationary state in quintic nonlinear optical media, *J. Opt. Soc. Amer. B* **14**, 2004-2009 (1997).
- [45] R. L. Pego and H. A. Warchall, Spectrally stable encapsulated vortices for nonlinear Schrödinger equations, *J. Nonlinear Sci.* **12**, 347-394 (2002).
- [46] T. A. Davydova and A. I. Yakimenko, Stable multicharged localized optical vortices in cubic-quintic nonlinear media, *J. Opt. A: Pure Appl. Opt.* **6**, S197 (2004).
- [47] X. Gao and J. Zeng, Two-dimensional matter-wave solitons and vortices in competing cubic-quintic nonlinear lattices, *Frontiers of Phys.* **13**, 130501 (2018).
- [48] D. Mihalache, D. Mazilu, L.-C. Crasovan, I. Towers, A. V. Buryak, B. A. Malomed, L. Torner, J. P. Torres, and F. Lederer, Stable spinning optical solitons in three dimensions, *Phys. Rev. Lett.* **88**, 073902 (2002).
- [49] Y. Li, Z. Chen, Z. Luo, C. Huang, H. Tan, W. Pang, and B. A. Malomed, Two-dimensional vortex quantum droplets, *Phys. Rev. A* **98**, 063602 (2018).
- [50] Z. Lin, X. Xu, Z. Chen, Z. Yan, Z. Mai, B. Liu, Two-dimensional vortex quantum droplets get thick, *Commun. Nonlinear Sci. Numer. Simulat.*, **93**, 105536 (2021).
- [51] Y. V. Kartashov, B. A. Malomed, L. Tarruell, and L. Torner, Three-dimensional droplets of swirling superfluids, *Phys. Rev. A* **98**, 013612 (2018).
- [52] P. G. Kevrekidis, D. J. Frantzeskakis, R. Carretero-González, B. A. Malomed, and A. R. Bishop, Discrete solitons and vortices on anisotropic lattices, *Phys. Rev. E* **72**, 046613 (2005).
- [53] T. Mayteevarunyoo, B. A. Malomed, B. B. Baizakov, and M. Salerno, Matter-wave vortices and solitons in anisotropic optical lattices, *Physica D* **238**, 1439-1448 (2009).
- [54] G. Chen, H. Wang, and Z. Chen, Discrete vortices on anisotropic lattices, *Front. Phys.* **10**, 104206 (2015).
- [55] X. Jiang, Z. Fan, Z. Chen, W. Pang, Y. Li, and B. A. Malomed, Two-dimensional solitons in dipolar Bose-Einstein condensates with spin-orbit coupling, *Phys. Rev. A* **93**, 023633 (2016).
- [56] Y. Li, Y. Liu, Z. Fan, W. Pang, S. Fu, and B. A. Malomed, Two-dimensional dipolar gap solitons in free space with spin-orbit coupling, *Phys. Rev. A* **95**, 063613 (2017).
- [57] B. Liao, S. Li, C. Huang, Z. Luo, W. Pang, H. Tan, B. A. Malomed, and Y. Li, Anisotropic semivortices in dipolar spinor condensates controlled by Zeeman splitting, *Phys. Rev. A* **96**, 043613 (2017).
- [58] X. Zhang, X. Xu, Y. Zheng, Z. Chen, B. Liu, C. Huang, B. A. Malomed, Y. Li, Semidiscrete quantum droplets and vortices, *Phys. Rev. Lett.* **123**, 133901 (2019).
- [59] A. B. Aceves, C. De Angelis, A. M. Rubenchik, and S. K. Turitsyn, Multidimensional solitons in fiber arrays, *Opt. Lett.* **19**, 329 (1994).
- [60] N. C. Panoiu, R. M. Osgood, B. A. Malomed, Semidiscrete composite solitons in arrays of quadratically nonlinear waveguides, *Opt. Lett.* **31**, 1097 (2006).
- [61] P. A. Subha, C. P. Jisha and V. C. Kuriakose, Stable diffraction managed spatial soliton in bulk cubic-quintic media, *J. Mod. Opt.* **54**, 1287 (2007).
- [62] A. Couairon and A. Mysyrowicz, Femtosecond filamentation in transparent media, *Phys. Reports* **441**, 47-189 (2007).
- [63] A. B. Aceves, C. De Angelis, G. G. Luther, and A. M. Rubenchik, Modulational instability of continuous waves and one-dimensional temporal solitons in fiber arrays, *Opt. Lett.* **19**, 1186 (1994).
- [64] A. B. Aceves, G. G. Luther, C. De Angelis, A. M. Rubenchik, and S. K. Turitsyn, Energy localization in nonlinear fiber arrays: Collapse-effect compressor, *Phys. Rev. Lett.* **75**, 73 (1995).
- [65] A. B. Aceves, C. De Angelis, G. G. Luther, A. M. Rubenchik, and S. K. Turitsyn, All-optical-switching and pulse amplification and steering in nonlinear fiber arrays, *Physica D* **87**, 262 (1995).
- [66] S. K. Turitsyn, A. M. Rubenchik, M. P. Fedoruk, and E. Tkachenko, Coherent propagation and energy transfer in low-dimension nonlinear arrays, *Phys. Rev. A* **86**, 031804(R) (2012).
- [67] R. Blit and B. A. Malomed, Propagation and collisions of semi-discrete solitons in arrayed and stacked waveguides, *Phys. Rev. A* **86**, 043841 (2012).
- [68] C. Chong, R. Carretero-González, B. A. Malomed, and P. G. Kevrekidis, Multistable solitons in higher-dimensional cubic-quintic nonlinear Schrödinger lattices, *Physica D* **238**, 126-136 (2009).
- [69] R. Driben, B. A. Malomed, A. Gubeskys, and J. Zyss, Cubic-quintic solitons in the checkerboard potential, *Phys. Rev. E* **76**, 066604 (2007).
- [70] S. Couris, M. Renard, O. Faucher, B. Lavorel, R. Chaux, E. Koudoumas, X. Michaut, An experimental investigation of the nonlinear refractive index (n_2) of carbon disulfide and toluene by spectral shearing interferometry and z -scan techniques, *Chem. Phys. Lett.* **369** 318 (2003).
- [71] D. Kong, Q. Chang, H. Ye, Y. Gao, Y. Wang, X. Zhang, K. Yang, W. Wu, and Y. Song, The fifth-order nonlinearity of

- CS₂, J. Phys. B, **42**, 065401 (2009).
- [72] J. Yang and T. I. Lakoba, Universally-convergent squared-operator iteration methods for solitary waves in general nonlinear wave equations, Stud. Appl. Math. **118**, 153 (2007).
- [73] L. Dong, W. Qi, P. Peng, L. Wang, H. Zhou, C. Huang. Nonlinear Dyn. **102**, 303 (2020).
- [74] N. G. Vakhitov and A. A. Kolokolov, Stationary solutions of the wave equation in a medium with nonlinearity saturation, Radiophys. Quantum Electron. **16** 783 (1973).